Spectrochimica Acta Part A: Molecular and Biomolecular Spectroscopy 329 (2025) 125567

Contents lists available at ScienceDirect

Spectrochimica Acta Part A:
Molecular and Biomolecular Spectroscopy

journal homepage: www.journals.elsevier.com/spectrochimica-acta-part-a-molecular-and-biomolecular-spectroscopy

Assessment of methodologies based on the formation of antiparallel triplex DNA structures and fluorescent silver nanoclusters for the detection of pyrimidine-rich sequences

Carlos Poyato [a], Javier Pacheco [a], Arnau Domínguez [b], Ramon Eritja [b], Anna Aviñó [b,*], Raimundo Gargallo [a,*]

[a] Dept. of Chemical Engineering and Analytical Chemistry, University of Barcelona, Marti i Franquès 1-11, E-08028 Barcelona, Spain
[b] Institute for Advanced Chemistry of Catalonia (IQAC-CSIC), CIBER-BBN, Jordi Girona 18-26, E-08034 Barcelona, Spain

HIGHLIGHTS

- Comparison of strategies based on duplex and antiparallel triplex formation.
- Assessment of antiparallel triplex formation by spectroscopy and Chemometrics.
- Detection of pyrimidine-rich sequences showing mismatches.

GRAPHICAL ABSTRACT

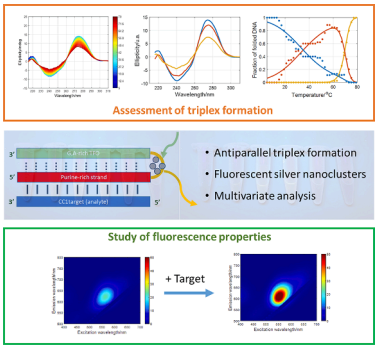

ARTICLE INFO

Keywords:
Antiparallel triplex DNA
Silver nanoclusters
Fluorescence
DNA detection
Melting experiments
Multivariate curve resolution

ABSTRACT

In this work, strategies for the detection of pyrimidine-rich DNA target sequences based on the formation of duplex and antiparallel triplex structures are studied. The presence of the target is detected from the changes in fluorescence of silver nanoclusters stabilized by the corresponding complementary DNA probes. In all cases, the formation of intermolecular structures has been assessed by means of melting experiments and multivariate analysis.

In the case studied, it has been observed that the formation of antiparallel triplex structures produces changes in fluorescence properties that could be more useful for analytical purposes than those observed when only duplex structures are formed. In particular, the use of silver nanoclusters confined within a loop rich in cytosine-type bases in the antiparallel triplex structure resulting from the interaction of probe and analyte has been shown to produce an increase in red fluorescence. This latter probe has been shown to be selective against target sequences that have mismatches that could affect the formation of stable duplex structures, while it has been shown to tolerate a small number of purine mismatches that could affect the stability of the resulting antiparallel triplex structure. As a final remark, it should be noted that this methodology could also be used in the

* Corresponding authors.
E-mail addresses: aaagma@cid.csic.es (A. Aviñó), raimon_gargallo@ub.edu (R. Gargallo).

https://doi.org/10.1016/j.saa.2024.125567
Received 10 September 2024; Received in revised form 11 November 2024; Accepted 3 December 2024
Available online 7 December 2024

development of analytical procedures that allow the detection of antiparallel triplex structures, which are difficult to observe with other spectroscopic methods.

1. Introduction

Nucleic acids may adopt a wide variety of spatial structures, including duplex (A-DNA, B-DNA…), G-quadruplex, i-motifs, and triplex, among others. Typically, nucleic acid triplex structures are formed in homopurine-homopyrimidine sequences of duplex DNA by interaction with a single-stranded triplex-forming oligonucleotide (TFO). This binds to the major groove of the Watson-Crick double-helical DNA by means of Hoogsteen hydrogen bonding [1,2]. The use of triplex structures has been suggested for therapeutics applications [3,4] or for diagnosis [5–8]. Overall, triplex structures may be classified into parallel and antiparallel triplexes according to the relative direction of the TFO in relation to the complementary purine-rich strand [1]. In the parallel triplex, a pyrimidine-rich TFO binds parallel to the homopurine strand within the duplex via Hoogsteen base pairs (Fig. 1a). Protonation of cytosine bases is required for the formation of stable Hoogsteen base pair between cytosine and guanine bases. For this reason, the stability of parallel triplex is pH-dependent being more stable in acidic pH, near the pK_a of cytosine [1]. In antiparallel triplex, the TFO is made of purine bases, and it binds antiparallel to the homopurine strand within the duplex via reverse Hoogsteen base pairs (Fig. 1b). In this case, there is no protonation to establish hydrogen bonds between bases and, consequently, its stability is pH independent (Fig. 1c). In general, parallel triplexes have been more studied from the structural and biochemical point of view than antiparallel triplexes because they show clear hypochromic changes in the UV spectra at 260 nm upon triplex formation, which can be used to follow the association or dissociation of the TFO.

Metal nanoclusters (NCs) are an important contribution of Nanotechnology to Nanomedicine due to their excellent physical and chemical properties [9]. NCs are tiny (below 2 nm) aggregations of a few metal atoms that have quantized molecule-like orbitals, enabling the measurement of fluorescence [10,11]. Extensive and critical reviews on this topic have been published [12–14]. In solution, NCs tend to form larger aggregates, known as nanoparticles (NPs), which have different properties to those shown by NCs. As example, NPs are not fluorescent, which hinders their use in analysis. To prevent this aggregation, different additives have been proposed [9,15]. Among them, DNA strands have been shown to be an easy and efficient way to stabilize NCs. As example, the fluorescence of adenine-templated gold nanoclusters has been shown to be useful for the determination of melanine [16]. Adenine and thymine-rich DNA have been also proposed for the determination of tetracycline by monitoring the changes in the fluorescence of copper nanoclusters [17]. Among DNA-stabilized NCs, most of the research has been done on silver nanoclusters (AgNCs) [18,19]. Ag(I) has more affinity with DNA bases than with the phosphate backbone, so they interact with the bases, to which they bond covalently. Affinity between DNA bases and Ag(I) can be enhanced by adding Mg(II) to neutralize the negative charges of the phosphate groups, reducing ionic interactions between Ag(I) and negatively charged phosphate groups. DNA-templated AgNCs provide an ideal platform for analysis of DNA and RNA sequences, thanks to their wide range and adjust ability of emitted fluorescence wavelength [20]. They have been proposed for the detection of single nucleotide polymorphisms and abasic sites [21], microRNAs [22,23], viral genomes [24], or for their antibacterial

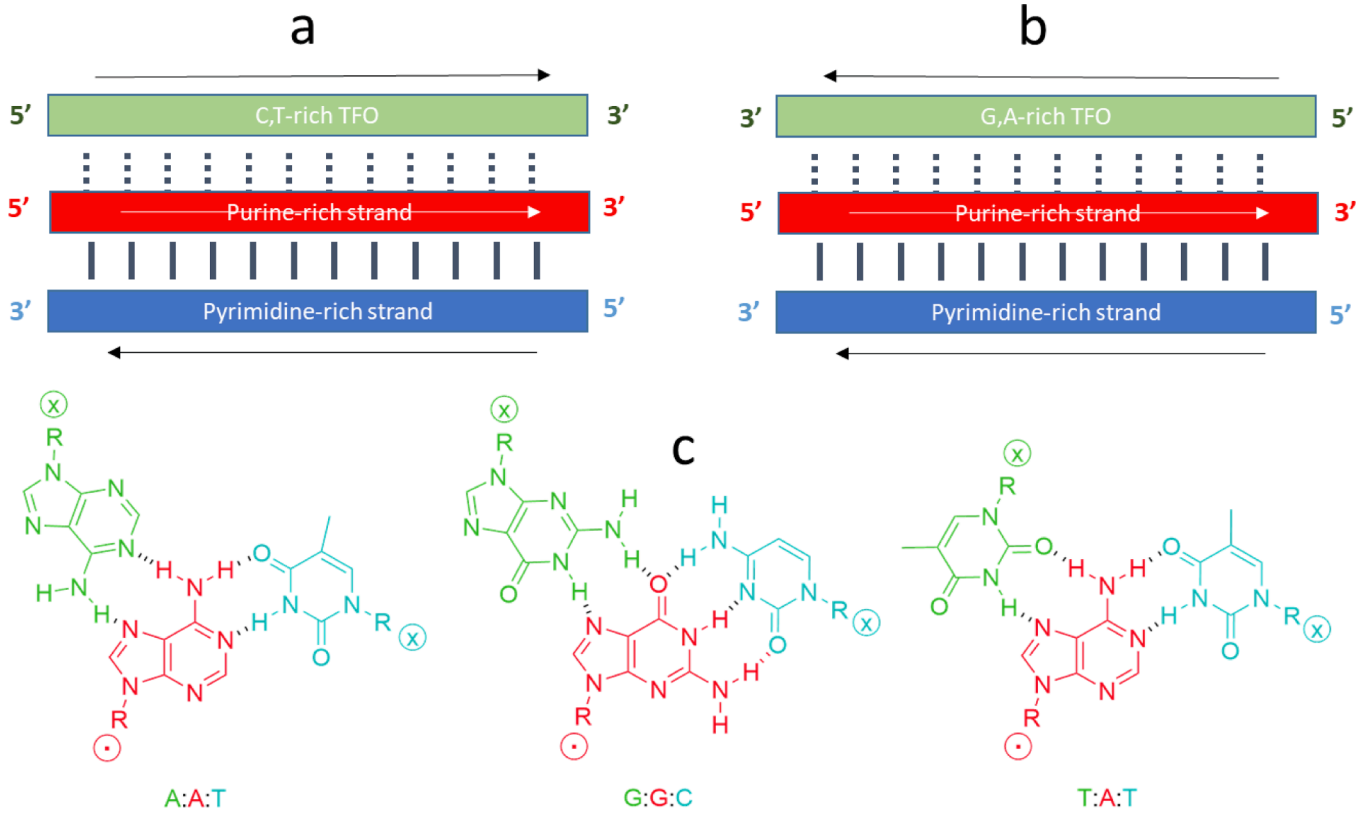

Fig. 1. (a) Scheme of a generic parallel triplex formed by two pyrimidine-rich sequences and a purine-rich strand. (b) Scheme of a generic antiparallel triplex formed by two purine-rich sequences and a pyrimidine-rich strand. (c) Hydrogen bonding scheme of the triads present in antiparallel triplex DNA. Solid lines indicate Watson-Crick hydrogen bonds, whereas dotted lines indicate non-Watson-Crick hydrogen bonds. Arrows indicate the 5′ to 3′ orientation of strands.

properties [25].

In a previous work, two different strategies based either on the formation of parallel or antiparallel triplex structures for the recognition of short stretches of C,T-rich DNA were assayed [26]. In the first case, the probe consisted of a hairpin stabilized by Watson-Crick hydrogen bonds, which was tagged at either the 3′ or 5′ end with a pyrimidine-rich DNA sequence able to stabilize fluorescent AgNCs. In this scheme, the recognition of the target would be based on the formation of a parallel triplex structure involving the hairpin and the target, which would function as a TFO. The formation of this triplex would produce a change in the fluorescence of the AgNCs attached to the probe. In practice, however, it was not observed any dramatic modification of the fluorescence that could be used to develop an analytical method based on this strategy. This could be due to the need of an acidic pH for the formation of parallel triplex structures, which could affect negatively to the fluorescence of AgNCs [27]. In the second strategy based on the formation of an antiparallel triplex structure, the probe consisted of purine-rich hairpins (or clamps) stabilized by reverse Hoogsteen hydrogen bonds. These clamps were labelled at the 3′ or 5′ extremes with the same tag sequence used in the parallel approach. In this second scheme, however, the recognition of the target was based on the formation of a duplex between the target and one of the strands of the probe, whereas the second purine-rich strand of the probe functioned as a TFO to yield an antiparallel triplex. It was observed that the formation of the triplex produced a modification of the fluorescence of the AgNCs, enabling the detection of the target.

Even though the strategy based on the formation of antiparallel triplex between the probe and the target pointed to a good starting point for the proposal of an analytical procedure, many questions remained unanswered. First, it was not clear the advantages (if any) of the strategy based on antiparallel triplex could have over a strategy based on the formation of the duplex between the target and the tagged complementary strand [22]. Second, other strategies based also on the formation of antiparallel triplex but not involving the use of a tag sequence could be explored. In this sense, it has been shown that the fluorescence of AgNCs encapsulated within a parallel triplex DNA structure with a cytosine-rich loop can be turned on and off in response to pH changes [28]. Hence, it could be of interest to evaluate whether a similar approach could be used, this time in the framework of antiparallel triplexes, for the recognition of a DNA target. Finally, the method was only evaluated for a C,T-rich sequence that did not contain any purine mismatch. The presence of these mismatches in wild-type pyrimidine-rich stretches is the most usual situation and it affects to the stability of the resulting antiparallel triplex [1,3].

In the present work, the strategy is extended to the detection of longer pyrimidine-rich sequences including purine interruptions. We have focused our attention on a 21 nucleotides long pyrimidine-rich stretch (CC1Target) found in the genome of SARS-CoV-2 [29,30]. The strategy based on the formation of antiparallel triplex structures is compared with that based on the formation of Watson-Crick duplexes. For this purpose, several instrumental techniques and experimental procedures have been applied, including molecular fluorescence and circular dichroism spectroscopies, or liquid chromatography, as well as multivariate data analysis.

2. Experimental

2.1. Reagents and solutions

Sigma-Aldrich (Merck KGaA, Germany) provided the DNA oligonucleotides (Table 1 and Fig. 2). The integrity of all DNA oligonucleotides was checked by means of MALDI-TOF Mass Spectrometry. DNA strand concentration was determined by absorbance measurements (260 nm) at 90 °C using the extinction coefficients calculated using the nearest-neighbor method as implemented on the OligoCalc webpage [31]. Potassium phosphate (pH 7.1) buffer, $AgNO_3$ and $NaBH_4$ were purchased from Merck KGaA. MilliQ (Merck Millipore, MA, USA) water was used in all experiments.

Table 1
DNA sequences used in this work. The colors follow the scheme shown in Fig. 2. Single underlined purine nucleotides indicate interruptions affecting the stability of the resulting antiparallel triplex, whereas double underlined nucleotides indicate mismatches affecting the stability of the resulting duplex.

DNA code	DNA sequence (5′ → 3′)	Length
CC1Target	**CTC TCT ACT ACC CTT CTG CTC**	21
CC1Target3MM	**CAC TCT AGT ACC CAT CTG CTC**	21
CC1TargetSCR	**TCT CCC GTC CAT TCC ACC TTT**	21
Tag	**CCC CTC AAT CCC**	12
TagCompWC	**CCC CTC AAT CCC GAG CAG AAG GGT AGT AGA GAG**	33
CompWCTag	**GAG CAG AAG GGT AGT AGA GAG CCC CTC AAT CCC**	33
TagCC1	**CCC CTC AAT CCC GAG CAG AAG GGT AGT AGA GAG** TTTT **GAG AGA TGA TGG GAA GAC GAG**	58
CC1Tag	**GAG CAG AAG GGT AGT AGA GAG** TTTT **GAG AGA TGA TGG GAA GAC GAG CCC CTC AAT CCC**	58
CC1_7C	**GAG CAG AAG GGT AGT AGA GAG CCCCCCC GAG AGA TGA TGG GAA GAC GAG**	49

The target (CC1Target) is a pyrimidine-rich sequence previously identified in the reverse strand of the SARS-CoV-2 viral genome and located at the replicase gene position 17,111 [29]. For this purpose, the Triplex-Forming Oligonucleotide Target Sequence Search software from University of Texas [32] was used. Parameters were set as follows: a minimum of 15 nucleotides in length, a minimum of 40 % GC content and a maximum of 3 pyrimidine interruptions, which have been underlined in the CC1Target sequence shown in Table 1. The presence of these three pyrimidine interruptions would not affect the stability of the duplex but could affect the stability of the resulting antiparallel triplex.

Most of the probes that will hybridize the CC1Target sequence contain a 12 nucleotides long tag sequence, denoted as Tag in the present work. The AgNCs stabilized by Tag have been shown to emit NIR fluorescence at certain experimental conditions [33]. The CC1Tag and TagCC1 probes are formed by a purine-rich clamp, denoted as CC1, and the Tag sequence attached at either the 3′ or 5′ end, respectively. It is expected that both probes will form antiparallel triplex structures in the presence of CC1Target according to the scheme shown in Fig. 2. The role of the TFO strand, shown in green in Fig. 2 and Table 1 will be evaluated by studying two probes (CompWCTag and TagCompWC) composed of the Tag sequence and the Watson-Crick forming duplex strand, i.e., in these oligonucleotides the TFO sequence has been removed.

The design of the CC1_7C probe is based on a slightly different approach. According to previous work [23], a Hoogsteen DNA parallel triplex structure with a seven-cytosine loop can encapsulate red fluorescent AgNCs, whose fluorescence is pH-dependent. We hypothesize that the fluorescence of these encapsulated AgNCs will be affected by the formation of triplex structures. Finally, in addition to the CC1Target sequence, two others (CC1Target3MM and CC1TargetSCR) have been designed. CC1Target3MM incorporates three additional mismatches that would negatively affect Watson-Crick base pair stability, while CC1TargetSCR is a random sequence with the same nucleotides as CC1Target.

2.2. Instruments and apparatus

Absorbance spectra were recorded with an Agilent 8453 diode array spectrophotometer. Hellma quartz cells (10 mm path length, 400 and 1500 μl volume, Germany) were used. CD spectra were recorded with a Jasco J-815 (MD, USA) spectropolarimeter equipped with a Peltier accessory for temperature control. Hellma quartz cells (10 mm path length, 3000 μl volume) were used.

Fluorescence experiments were monitored using an AB2 Aminco-Bowman (Thermo Fisher, MA, USA) spectrofluorimeter. For most of

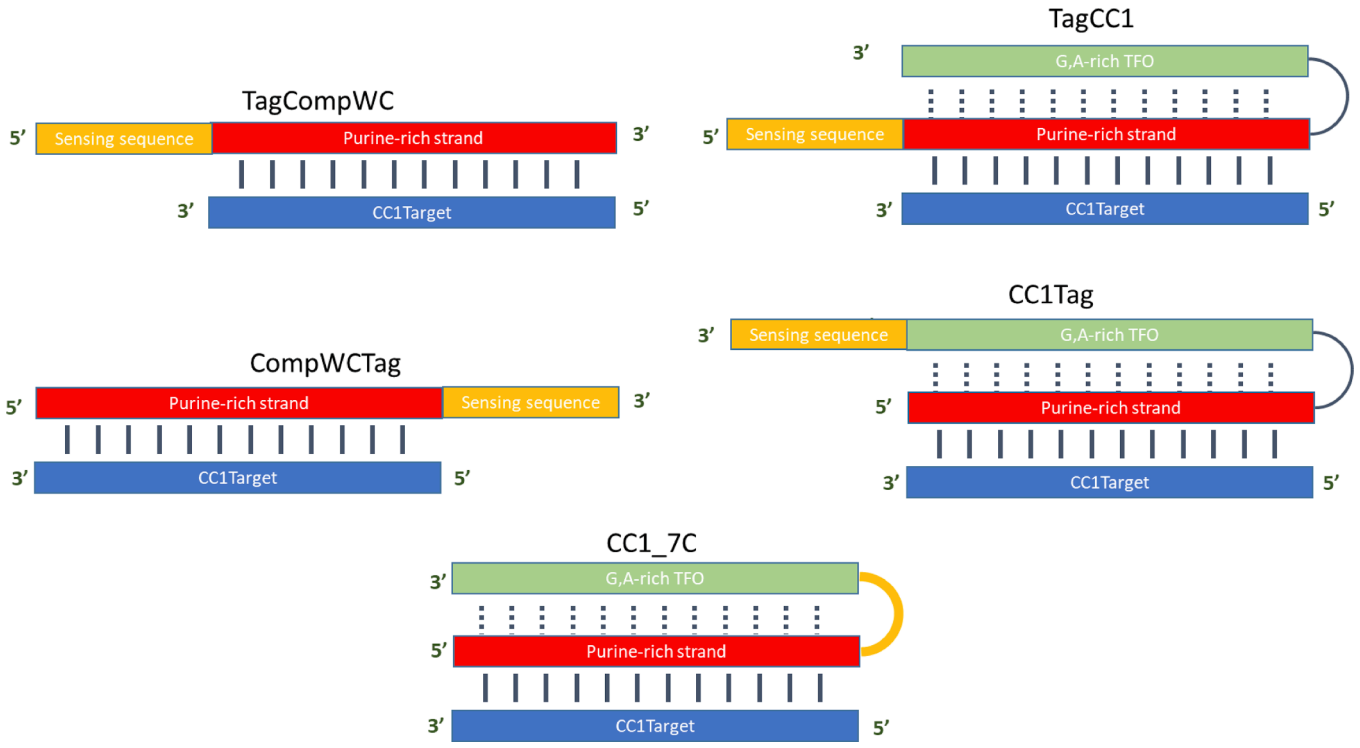

Fig. 2. Intermolecular structures proposed for the interaction of CC1Target with the duplex- and triplex-forming oligonucleotides listed in Table 1. Solid black lines indicate Watson-Crick-type base pairs, whereas dotted black lines indicate reverse Hoogsteen-type base pairs. Solid yellow line in CC1_7C indicates the seven cytosines loop. Polypyrimidine target, polypurine Watson-Crick and polypurine TFO are represented in blue, red, and green, respectively.

the measurements, excitation and emission slits were set to 4 nm, and voltage of the photomultiplier was set to 600 V. A Hellma quartz cell (2 x 10 mm path length, and 400 μl volume) was used.

For reverse phase HPLC-UV, the chromatographic system consisted of a Waters 2695 HPLC instrument equipped with a quaternary pump, a degasser, an autosampler, and a photodiode-array detector, and software for data acquisition and analysis. The chromatographic column used for separation at room temperature was a Symmetry C18 (100 Å, 5 μm, 4.6 mm × 250 mm, Waters). The compositions of mobile phases were acetonitrile:0.1 M triethylammonium acetate (5:95, mobile phase A) and acetonitrile:0.1 M triethylammonium acetate (70:30, mobile phase B). A gradient from 100:0 (phase A:phase B) to 50:50 in 20 min was used for the separation. The flow rate was set to 0.8 mL min^{-1}. The injection volume was 15 μL.

2.3. Procedures

Melting experiments were performed using DNA solutions in 20 mM cacodylate buffer (pH 7.1) and 50 mM magnesium nitrate, previously annealed overnight. These solutions were transferred to the cell and allowed to equilibrate at the initial temperature for 15 min. Ellipticity was measured at 275 nm, whereas spectra (210–310 nm) were measured every 2 °C, being the heating rate 0.5 °C min^{-1}. The blank was removed, and the spectra were smoothed by applying a Savitzky-Golay filter.

3D excitation-emission fluorescence maps (EEMs) were measured from 400 to 700 nm (excitation), and from 500 to 800 nm (emission). The Rayleigh scattering was removed by replacing the original values by an estimate of the background fluorescence signal. This estimate was calculated from the mean value of a wide region of the EEM where no fluorescence was observed, and later addition of random noise. Finally, the EEM was smoothed by applying a Savitzky-Golay filter. All these procedures were done using in-house developed Matlab® (The MathWorks, Inc., MA, USA) routines. The following visible spectral ranges were considered along the manuscript: green (501–565 nm), yellow (566–590 nm), orange (591–625 nm), and red (626–740 nm).

The general procedure used throughout this work for the synthesis of DNA-AgNCs and subsequent measurement of EEM in the absence and presence of the target is shown in Fig. S1 (blue route) [34]. In vials containing the appropriate medium (20 mM cacodylate buffer, pH 7.1, 50 mM magnesium nitrate), aliquots of the probe stock solution were introduced. A certain volume of $AgNO_3$ was then added to achieve a 1:6 DNA:Ag(I) molar ratio, the mixture was shaken and allowed to stand for 15 min at room temperature and in the dark. Then, freshly prepared $NaBH_4$ was added to the DNA:Ag(I) mixture up to a 1:6:6 DNA:Ag(I):borohydride molar ratio, and the solution was stirred vigorously for 1 min. The synthesized DNA-AgNCs were stored at 4 °C in the dark for one hour before EEM measurement. For the measurement in presence of the target, the whole procedure was repeated using a 1:1 target:probe mixture. The 1:6:6 ratio was again referred to the concentration of probe. For both samples, probe and mixture, the entire procedure was performed in duplicate. As will be described below, an alternative approach was also assessed in which the target was added to the previously synthesized AgNC-probe (Fig. S1, orange route). In this case, the mixture was kept for 5 min in the dark before the measurement.

In all procedures, the $AgNO_3$ stock solution was prepared by dissolving in a 10 mL volumetric flask the mass of $AgNO_3$ required to obtain a 0.1 M concentration solution. A $1{\cdot}10^{-3}$ M $AgNO_3$ solution was obtained through a dilution cascade, which was stored at room temperature in an amber volumetric flask to prevent oxidation. The $NaBH_4$ stock solution was prepared daily by dissolving the appropriate amount of solid $NaBH_4$ in a 25 mL volumetric flask to obtain a 0.1 M solution. From this, a $1{\cdot}10^{-3}$ M $NaBH_4$ solution was obtained by dilution, which was kept on ice until use.

2.4. Data analysis

CD-monitored melting experiments provided not only ellipticity *vs.* temperature at a one single wavelength, but also a CD spectrum every

2 °C from 5 to 80 °C. The measured spectra along a melting experiment were arranged in a data matrix that was later analyzed by means of the Multivariate Curve Resolution – Alternating Least Squares (MCR-ALS) method. Briefly, this method allows the determination of the number of components present along the melting (which have been assigned to different folded conformations), as well as their corresponding concentration profiles and pure CD spectra. The method has been applied successfully to many biophysical and analytical studies, such as the analysis of melting experiments [29,35], the interaction of drugs and DNA [36], or the separation of i-motif structures by capillary electrophoresis [37] or HPLC analysis [38], among others. Extensive information on the method is given in those articles.

3. Results

As stated above, the first objective of this work is to investigate the potential advantages of the antiparallel triplex-forming strategy for the recognition of pyrimidine-rich sequences using fluorescent AgNCs over the strategy based on the formation of duplex structures. Because of this, the application of this last strategy for the recognition of a target pyrimidine-rich sequence (CC1Target) will be presented first. Then, the formation of antiparallel triplex structures involving this target and several probes will be assessed. Finally, the basis of a detection method based on fluorescence changes due to the formation of triplex structures will be presented and discussed.

3.1. Detection of pyrimidine-rich DNA using complementary tagged probes

In a previous work, Yang and Vosch proposed an analytical procedure for the detection of microRNAs [22]. This was based on the quantitative reduction of the fluorescence of a probe after its hybridization with the target to yield a Watson-Crick stabilized duplex. The fluorescent probe was formed by the complementary strand tagged at its 5′ end with a short, cytosine-rich DNA sensing sequence prone to stabilize fluorescent AgNCs. Upon formation of the duplex structure, the fluorescence of the AgNCs decreased allowing the detection of the microRNAs. In this work, we have explored the application of this strategy using the TagCompWC and CompWCTag sequences, which are able to form a duplex with the CC1Target, and which contain a AgNC-forming tag sequence at the 5′ and 3′ ends, respectively (Table 1 and Fig. 2).

Before the fluorescence measurements, the formation of stable duplex structures between each one of these probe sequences and the CC1Target was assessed by means of CD-monitored melting experiments of each one of these sequences, as well as those corresponding to the 1:1 mixtures (Figs. 3 and S2, and Table 2). First, the melting curve of CC1Target alone was analyzed (Fig. S2a). The shape of the spectrum at 5 °C is characterized by a positive signal around 275 nm and a weak and broad negative signal centered at 245 nm, which are lost smoothly upon heating. All together, these features pointed to a little ordered structure at low temperatures and pH 7.1, in agreement with the base composition of this sequence. For TagCompWC, the picture is different to that observed for CC1Target (Fig. 3a). The CD spectrum of TagCompWC at 5 °C is characterized by intense positive and negative signals at 270 and 240 nm, respectively, which change dramatically upon heating. This points out to the existence of an initial partially ordered structure, as predicted by *in silico* analysis [39,40] (Fig. S3). Multivariate analysis based on MCR-ALS has been applied to the analysis of all CD spectra measured along the melting experiment. The result of this analysis supports the assumption of a two-step unfolding process with a T_m value equal to 43 ± 1 °C. (Fig. 3b and 3c).

Table 2
Melting temperatures (T_m) values from CD-monitored denaturation experiments. Experimental conditions were 1 μM DNA strand, 20 mM cacodylate buffer (pH 7.1), 50 mM magnesium chloride.

DNA strand	Without CC1Target (T_m °C)	With CC1Target (T_m °C)	
		Triplex → duplex	duplex → single strands
TagCompWC	43 ± 1		69.8 ± 0.5
CompWCTag	39 ± 1; 59 ± 1		69.4 ± 0.5
TagCC1	40.6 ± 0.5	32 ± 1	64 ± 1
CC1Tag	40.5 ± 0.7	32 ± 1	65 ± 1
CC1_7C	45.9 ± 0.8	34 ± 2	70.7 ± 0.6

Next, the melting curve of the 1:1 TagCompWC+CC1Target mixture was analyzed. The CD spectrum at 5 °C showed spectral characteristics that are slightly different from that of TagCompWC (Fig. 3d). The analysis of the CD trace at 275 nm showed a cooperative transition at 69.8 ± 0.5 °C (not shown), which was assigned to the disruption of the Watson-Crick duplex formed by these two sequences. Multivariate analysis showed that the whole unfolding process should be explained considering three components (Fig. 3e and f). The second transition, which takes place at 69.8 ± 0.5 °C, is clearly related to the denaturation of the duplex structure, whereas the first transition, which involves a small spectral change, could be related to the unfolding of a minor contribution of TagCompWC not involved in the duplex.

Concerning the melting of the CompWCTag strand (Fig. S2b), the analysis of the ellipticity at 275 nm *vs.* T curve suggested a two-state unfolding with a T_m equal to 38.4 ± 0.6 °C (not shown). However, a wider look considering the whole CD spectra and appropriate multivariate data analysis demonstrated that the complete unfolding takes place in two steps with T_m values equal to 39 and 59 °C (Fig. S2c and d). The differences between the meltings of TagCompWC and CompWCTag could be related to the relative stabilities of the predicted structures at 15 °C (20 mM Na^+ and 50 mM Mg^{2+}). Hence, whereas the Gibbs free energies for the two most stable predicted structures for TagCompWC were −4.5 and −4.0 kcal·mol^{-1}, the values for the two most stable predicted structures for CompWCTag were −4.0 and −3.7 kcal·mol^{-1}, respectively (Fig. S3). Therefore, not only TagCompWC oligonucleotide forms the most stable structure in terms of Gibbs free energy, but also CompWCTag is predicted to fold into a mixture of structures with more similar stabilities (0.3 kcal·mol^{-1}) than in the case of TagCompWC (0.5 kcal·mol^{-1}). Finally, the melting of the 1:1 CompWCTag:CC1Target was well-modelled considering only one strongly cooperative transition at 69.4 ± 0.3 °C, which obviously was related to the disruption of the duplex (Fig. S2f and g). All together, these experiments confirmed the formation of similar and very stable duplex structures between the considered probes and the CC1Target at 15 °C.

Next step was the study of the fluorescence of AgNCs stabilized by TagCompWC and CompWCTag probes, and how it is modified upon the corresponding interaction with the CC1Target. First, it was measured the EEM of the 12 nucleotides long Tag sequence, which shows strong orange fluorescence at 620 nm, together with weaker green and red fluorescence at 520 and 690 nm (Fig. S4). This different emission suggests the existence of several AgNCs with a different number of Ag(I) and Ag(0) species. According to previous works, the fluorescence of AgNCs species would be strongly dependent on the ratio of Ag(I)/Ag(0) species [41], as well as on the size of the AgNCs [42]. Hence, it has been proposed that, in most of the species stabilized by different DNA templates, there are two types of dominant colors and Ag atom numbers, including near 540 nm with four atoms and 630 nm with six atoms [43], which roughly agree with the emission observed for Tag sequence.

Next, the fluorescence of the TagCompWC probe, which is based on the proposed strategy by Yang and Vosch [22], was measured. As the Tag sequence, the AgNCs stabilized by the TagCompWC also showed intense orange fluorescence at 620 nm, together with a weak fluorescence at 690 nm (Fig. 4a). However, no fluorescence was observed at 520 nm. Next, AgNCs were synthesized by adding silver nitrate and sodium borohydride to a 1:1 TagCompWC:CC1Target mixture (blue route in Fig. S1). The observed fluorescence of the AgNCs in the mixture

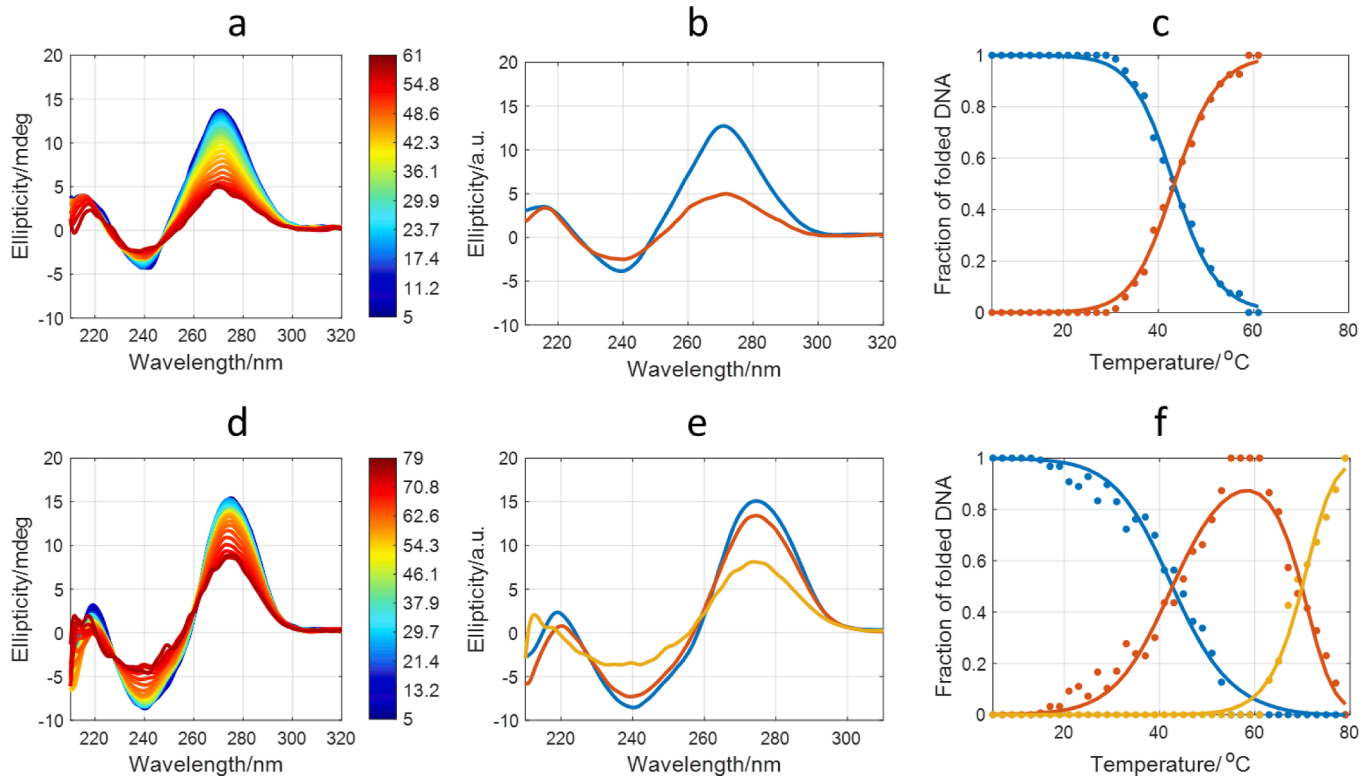

Fig. 3. Melting experiments of TagCompWC (a–c) and of the 1:1 mixture of TagCompWC:CC1Target (d–f). Pannels (a) and (d) show the spectra measured along the melting experiments. Pannels (b) and (e) show the MCR-ALS resolved pure spectra, whereas panels (c) and (f) show the MCR-ALS resolved distribution diagrams. Symbols in pannel (c) and (f) are the results obtained by MCR-ALS, whereas the fitted lines have been added for a better lecture of each pannel.

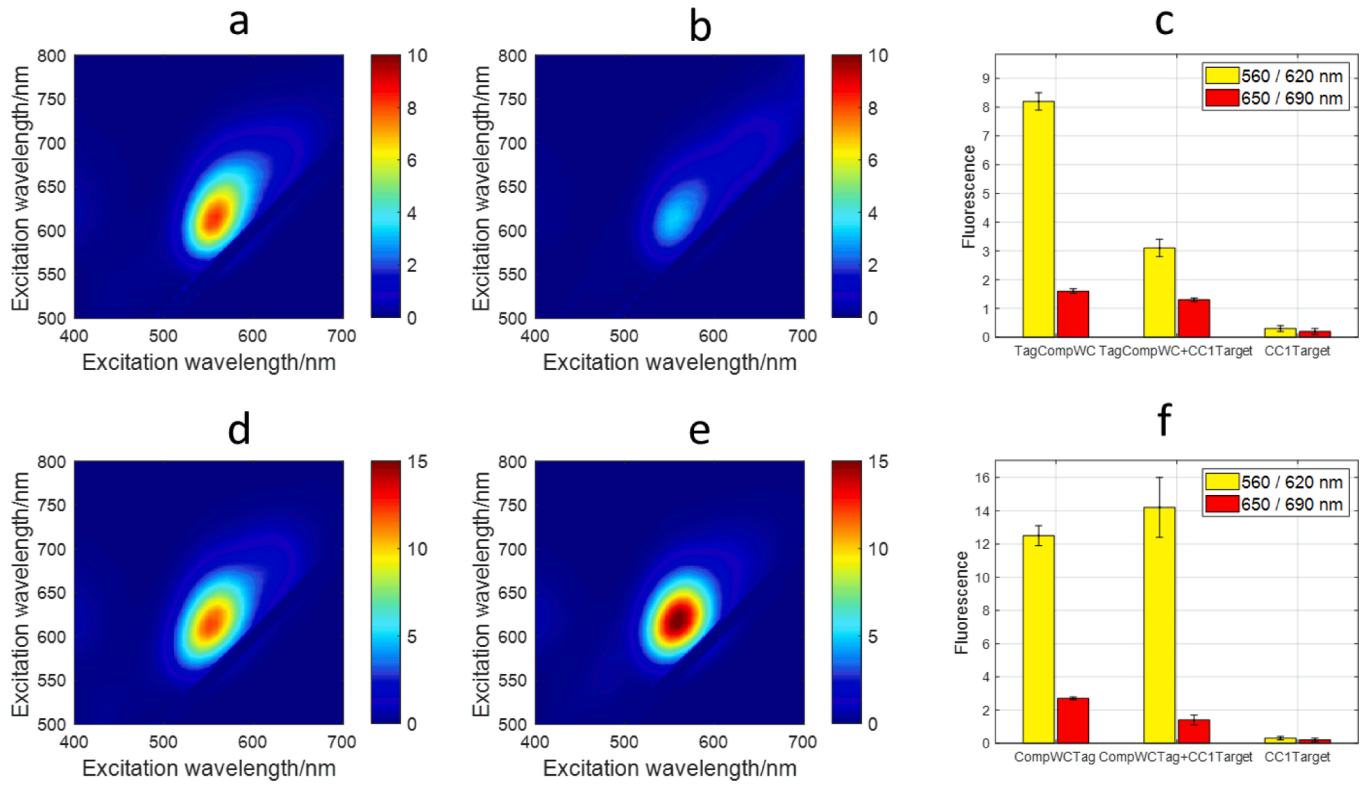

Fig. 4. EEMs of the probes (a, d) and 1:1 probe:target (b, e) based on the duplex-forming strategy (TagCompWC, 1st row, and CompWCTag, 2nd row) and comparison of the fluorescence intensities (c, f). In all cases, DNA strand, silver nitrate and sodium borohydride concentrations were 5, 30, and 30 μM, respectively. The concentration of CC1Target was also 5 μM in the mixtures. The solutions contained 20 mM cacodylate buffer (pH 7.1), and 50 mM magnesium chloride. Measurements were conducted at 15 °C.

(Fig. 4b and 4c) showed a 63 % reduction of the fluorescence at 620 nm in relation to that observed in absence of the target. This observation is in line with those previously described by Yang and Vosch. It should be stressed that the AgNCs potentially stabilized by the CC1Target did not show significant fluorescence at the same experimental and instrumental conditions (Fig. S5).

The CompWCTag-AgNC showed strong orange fluorescence at 620 nm, in a comparable way to that observed for the TagCompWC sequence (Fig. 4d). However, two main differences were observed. First, the fluorescence intensity of the CompWCTag-AgNC at this wavelength was 50 % higher than that of TagCompWC-AgNC. Secondly, the addition of the CC1Target did not produce any clear reduction of the fluorescence of CompWCTag-AgNC, which is a different situation to that shown for the TagCompWC probe. The reason for these differences between the fluorescent properties of these two probes could lie on a different folding of this oligonucleotides in presence of Ag species. Hence, it is deduced that the position (5′ or 3′) at which the Tag sequence is attached to the complementary strand may produce differences in the secondary structure of the probe, which in turn would produce differences in the spectral characteristics of the probe-stabilized AgNCs.

Even though the observed reduction of fluorescence is a way to detect, and even quantify, a target, more sensitive analytical methods are those developed based on the appearance of a net signal. In addition, it has been suggested that the formation of antiparallel triplex structures could be a way to increase the selectivity of a sequence towards its complementary strand [8,44]. Therefore, alternative approaches based on the formation of antiparallel triplex structures were assessed.

3.2. Assessment of the formation of antiparallel triplex structures by CD spectroscopy

First, the formation of triplex structures was studied by CD-monitored melting experiments of individual sequences and mixtures. Figs. 5 and S6 show the CD spectra measured along the melting experiments of all sequences and 1:1 mixtures, and Table 2 summarizes the results of the thermodynamic analysis.

For TagCC1, the intense CD spectra measured at low temperatures, as well as the clear unfolding observed upon increasing the temperature, pointed out to the existence of a well-ordered structure at low temperatures (Fig. 5a). Multivariate analysis allowed the definition of a single transition with T_m equal to 40.6 ± 0.5 oC (Fig. 5b and 5c). Even though the potential formation of internal hairpins cannot be ruled out, this transition has been assigned to the unfolding of an antiparallel duplex stabilized by reverse-Hoogsteen bonded base pairs, as suggested previously for the raw CC1 sequence (which lacks the Tag sequence) [29].

Upon addition of the CC1Target, subtle spectral changes were observed around 210 nm and at higher temperatures (Fig. 5d). Multivariate analysis allowed the resolution of two transitions along the melting process (Fig. 5e and 5f). The first transition, which takes place around 32 °C, has been related to the releasing of the TFO from the antiparallel triplex structure. The second transition, which takes place at 64 °C has been related to the disruption of the remaining duplex structure formed by CC1Target and one of the purine-rich strands in TagCC1 (Fig. 2). The small reduction of the T_m value in relation to those determined previously for the duplex formed by TagCompWC and CC1Target (69.8 °C) has been related to the destabilizing effect of the attached TFO strand, which fluctuates freely after being released from the triplex. On the other hand, the reduction of the T_m value of the first transition from 40.6 °C (for the TagCC1 duplex) to 32 °C (for the TagCC1:CC1Target triplex) has been related previously to the destabilization of the reverse Hoogsteen base pairs in the triplex because of the simultaneous presence of the Watson-Crick base pairs (Fig. 1) [29].

The melting experiments of CC1Tag and the corresponding 1:1 mixture with CC1Target provided comparable results to those shown for TagCC1 (Fig. S6 and Table 2). Overall, the melting experiments supported the formation of antiparallel triplex structures between the

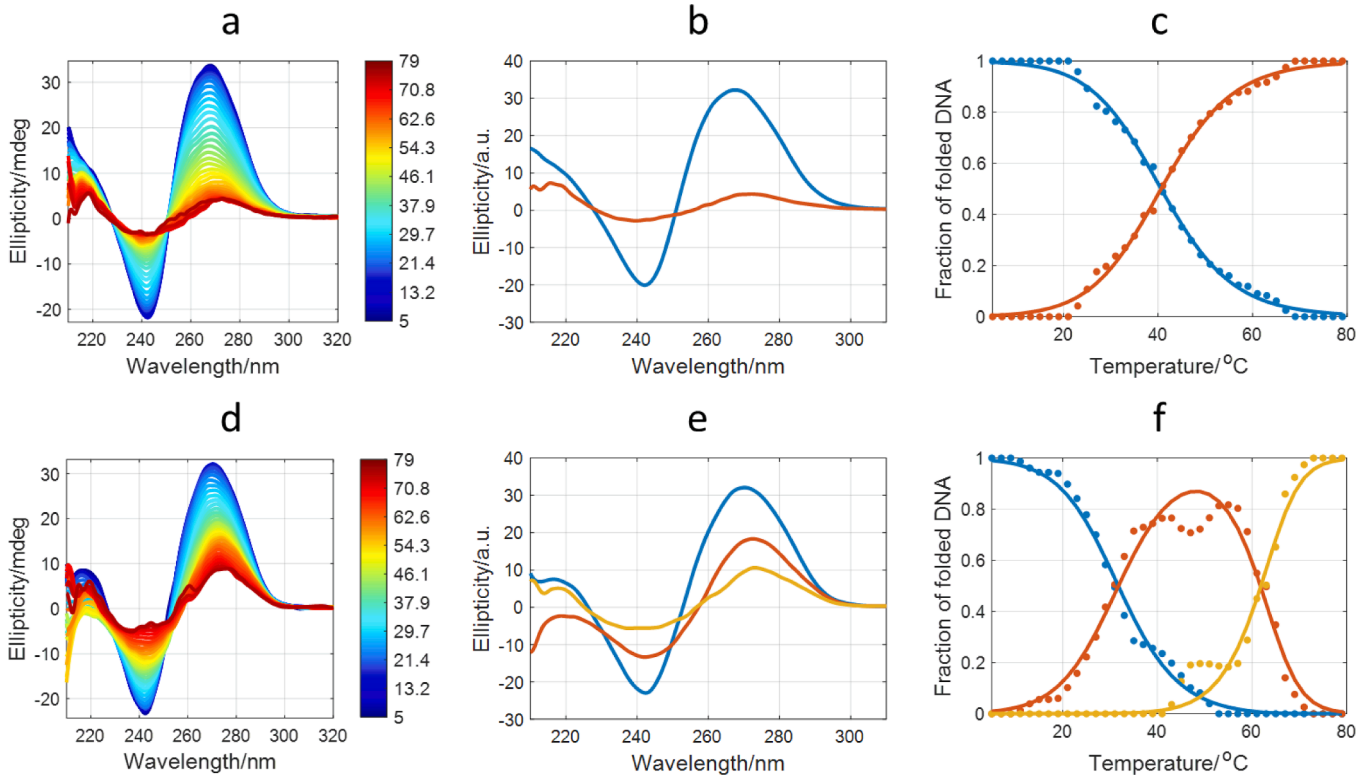

Fig. 5. Melting experiments of TagCC1 (a–c) and of the 1:1 mixture of TagCC1:CC1Target (d–f). Pannels (a) and (d) show the spectra measured along the melting experiment. Pannels (b) and (e) show the MCR-ALS resolved pure spectra, whereas panels (c) and (f) show the MCR-ALS resolved distribution diagrams. Symbols in pannel (c) and (f) are the results obtained by MCR-ALS, whereas the fitted lines have been added for a better lecture of each pannel.

probes and the CC1Target.

3.3. Detection of pyrimidine-rich DNA based on the formation of antiparallel tagged triplex structures

Fig. 6 shows the EEMs of the AgNCs stabilized by the TagCC1 and CC1Tag probes in absence and presence of the CC1Target. The EEM of TagCC1 probe showed strong orange fluorescence at 620 nm and residual fluorescence at 520 and 690 nm. This EEM is like that observed for the TagCompWC, which lacks the TFO strand. In presence of the CC1Target, a 77 % reduction of the orange fluorescence was observed. At this point, an alternative procedure was evaluated, where the CC1Target was added to the previously synthesized TagCC1-AgNCs (orange route in Fig. S1). This approach produced a 53 % reduction of orange fluorescence. Overall, the spectral features related to TagCC1, both in absence and presence of CC1Target, are like those observed for TagCompWC, revealing the negligible effect of the polypurine TFO on this scheme.

A different situation was observed for CC1Tag. In this case, the EEM of the CC1Tag-AgNC showed not only intense orange emission at 620 nm, but also a weak red fluorescence at 690 nm and residual green fluorescence at 520 nm. In presence of the CC1Target, the fluorescence intensity at 520 nm increased dramatically, whereas minor variation was observed at 620 nm. As in the case of TagCC1 approach showed above, more dramatic changes were observed when AgNCs were produced using the previously annealed mixture of CC1Tag and CC1Target (blue route in Fig. S1, "Mixture" in Fig. 6) than when adding the CC1Target to the AgNCs stabilized by CC1Tag (orange route in Fig. S1, "CC1Tag + CC1Target" in Fig. 6).

Overall, the behavior observed for CC1Tag is clearly different from that described for CompWCTag, a probe that hardly showed a 12 % reduction of the red fluorescence (Fig. 3). We hypothesized that these differences could be related to the relative position of the Tag sequence in both probes. In TagCC1, the Tag sequence is attached to the Watson-Crick polypurine strand, which interacts with both the CC1Target (forming Watson-Crick hydrogen bonds) and to the polypurine TFO (forming reverse-Hoogsteen hydrogen bonds) (Fig. 2). On the other hand, in CC1Tag the Tag sequence is attached to the polypurine TFO, which only interacts with the Watson-Crick polypurine strand forming reverse-Hoogsteen hydrogen bonds (Fig. 2). The different structural variations when the target binds to the probe and the stability of the hydrogen bonds that the strand directly attached to the Tag sequence is forming could explain these differences.

3.4. Detection of pyrimidine-rich DNA using a cytosine-rich loop antiparallel triplex

Until now, only the CC1Tag probe has shown the appearance of a strong new fluorescence in the presence of the CC1Target. However, the signal at 520 nm appears in the green region, where cellular and tissue autofluorescence may interfere in hypothetical *in vivo* application of these methods. At this point, the behavior of AgNCs confined within the cytosine-rich loop of an antiparallel triplex has been studied. To do this, an additional triplex-forming probe was tested (CC1_7C, Table 1), which includes a cytosine-rich loop that has been suggested to provide strong red fluorescence in Watson-Crick stabilized hairpins [28,45]. As in the previous cases, the thermal unfolding of CC1_7C and of the 1:1 CC1_7C: CC1Target mixture were studied firstly by means of CD spectroscopy and MCR-ALS analysis (Fig. S7). As in other cases, it was assessed the formation of a triplex structure at low temperatures with a T_m value equal to 34 ± 2 °C. This uncertainty was because the spectrum of the triplex hardly differs from that of the species that only forms duplex (Fig. S7e). This similarity produces a poorly defined distribution diagram (Fig. S7f) which, in turn, affects the determination of T_m.

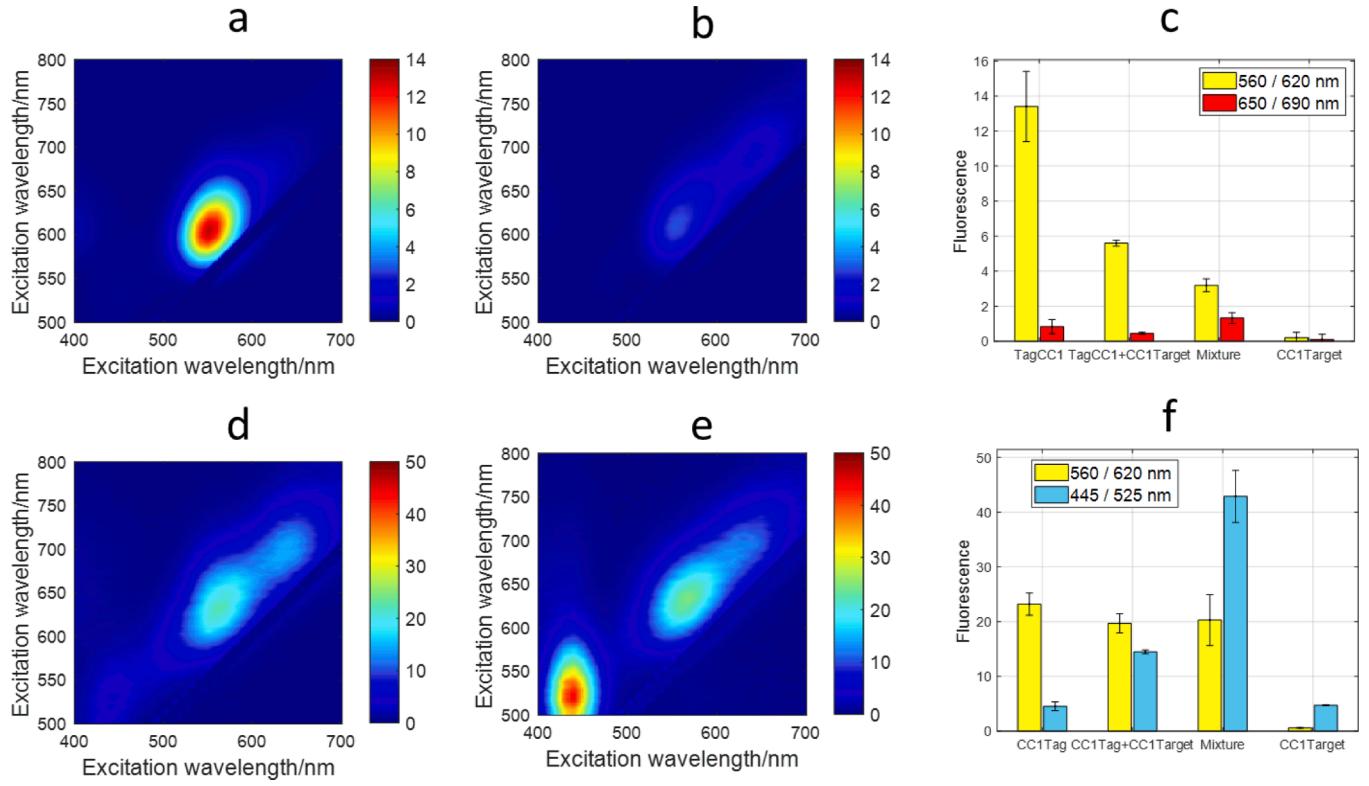

Fig. 6. EEM of the probes (a, d) and 1:1 probe:target mixtures (b, e) based on the antiparallel triplex-forming strategy (TagCC1, 1st row, and CC1Tag, 2nd row) and comparison of the fluorescence intensities (c, f). "Mixture" and "TagCC1 + CC1Target" refer to the blue and orange routes in Fig. S1, respectively. In all cases, DNA strand, silver nitrate and sodium borohydride concentrations were 5, 30, and 30 μM, respectively. The concentration of CC1Target was also 5 μM in the mixtures. The solutions contained 20 mM cacodylate buffer (pH 7.1), and 50 mM magnesium chloride. Measurements were conducted at 15 °C.

Concerning the fluorescence properties of the CC1_7C-AgNC, these present also a strong fluorescence around 620 nm (Fig. 7a and b). Interestingly, a 104 % increase of the fluorescence was observed in presence of the CC1Target, which would make this probe more suitable for the determination of pyrimidine-rich strands than TagCC1 (which shows a slight reduction of the orange fluorescence at 620 nm) or CC1Tag (which shows a dramatic increase of the green fluorescence at 520 nm).

The species related to the CC1_7C sequence were studied by HPLC-UV (Fig. 7c). The naked DNA showed a single peak at 8.52 min, with a small shoulder around 8.7 min. After the formation of the AgNCs, two peaks were observed at 8.52 and 8.77 min. According to previous literature, the presence of these two peaks could be related to the formation of dimer structures linked through the cytosine bases at the loops [45]. The peak at 8.52 min suggests that the hydrodynamic volume of the DNA within the AgNC ensemble is like that of naked DNA, as suggested by other authors based on CD spectroscopy measurements [46]. In this sense, the AgNCs stabilized by TagCompWC and TagCC1 also showed this behavior (Fig. S8).

Upon addition of the CC1Target, a major peak appeared at 9.21 min, with shoulder at 9.46, and minor signals at 8.56 and 8.9 min. This chromatogram is more complex than those recorded for the mixtures of AgNC-TagCompWC:CC1Target (which forms a duplex) or AgNC-TagCC1:CC1Target (which forms a triplex). Overall, the chromatogram indicates that the fluorescence signal of CC1_7C corresponds to a mixture of species.

From the different probes essayed, the CC1_7C-AgNC appears to produce the clearest changes in orange fluorescence upon interaction with CC1Target. The selectivity of this probe was studied by measuring the fluorescence produced in presence of two DNA sequences (CC1SCR and CC13MM) of similar composition to the CC1Target (Table 1). The CC1SCR is a scrambled sequence of equal composition than CC1Target, which should not produce any triplex structure in presence of CC1_7C. On the other hand, the CC13M sequence includes three additional mutations in relation to the CC1Target sequence that could produce destabilization of the resulting CC1_7C:CC1Target duplex structure. Fig. 7b shows the fluorescence measured in the presence of both sequences. It was observed that the CC1_7C-AgNC probe showed good selectivity against these two sequences.

4. Conclusions

As described in the introduction, the main objectives of this work were threefold: (i) to evaluate the potential advantages of the strategy based on antiparallel triplex formation versus that based on duplex formation, (ii) to explore other strategies that do not rely on the presence of a tagged sequence at the ends of the probe, and (iii), to test the methodology for sequences with mismatches that may affect duplex and triplex formation. The following conclusions can be drawn from the results obtained. First, the strategy based on the use of labeled probes capable of forming antiparallel triplex structures has shown clear advantages over the use of labeled probes capable of forming only duplex structures. Thus, both TagCC1 and CC1Tag have shown spectral changes after addition of the target, whereas only TagCompWC showed a reduction in orange fluorescence. Second, the use of AgNCs confined within a cytosine-rich loop within a clamp (CC1_7C probe) has been shown to be a useful tool for target recognition. Third, the approach has been shown to be selective in front of sequences showing mismatches that could affect the formation of stable duplex structures (CC1Target3MM and CC1TargetSCR), whereas it has been shown to handle a small number of purine mismatches that could affect the stability of the resulting antiparallel triplex structure (CC1Target). As a final remark, it should be noted that this methodology could also be used in the development of analytical procedures that allow the detection of antiparallel

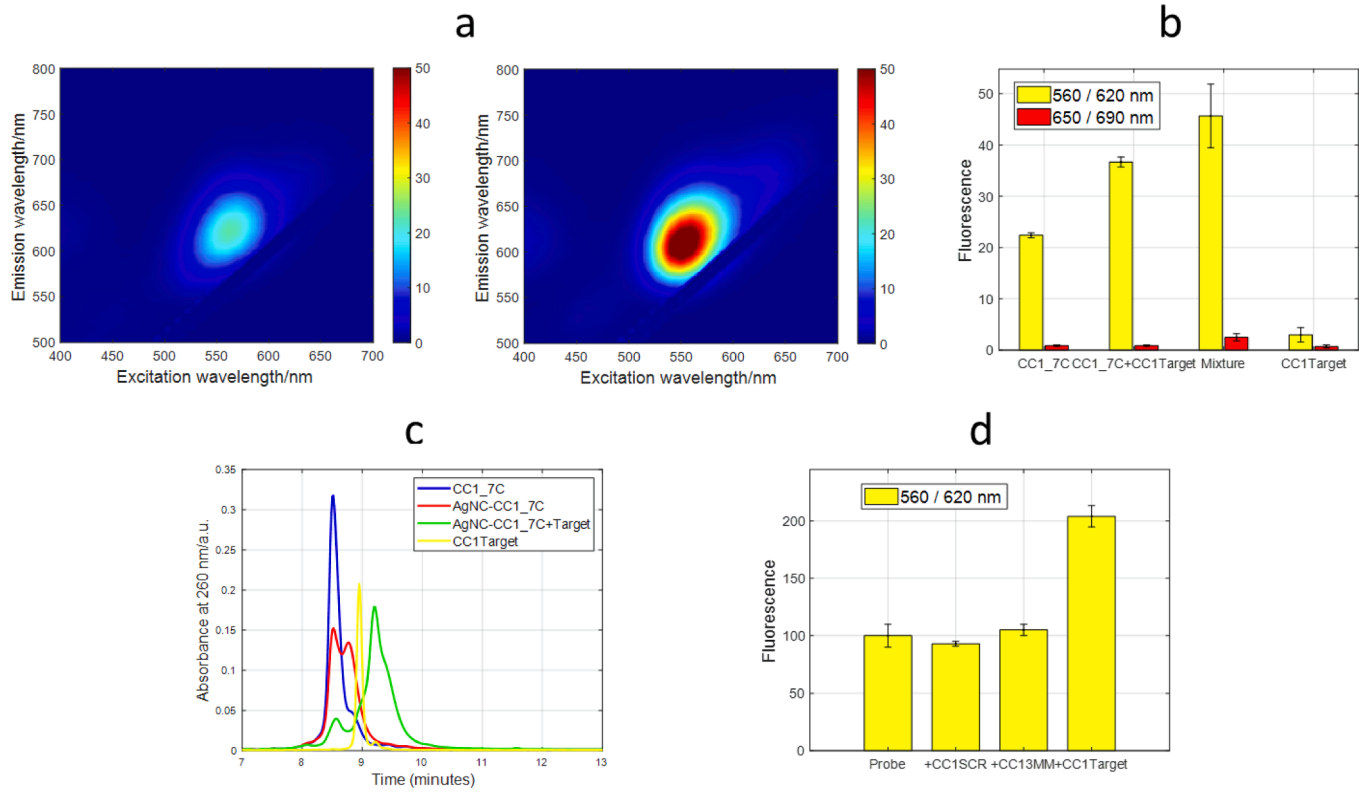

Fig. 7. (a) EEM of the probes and 1:1 probe:target based on the antiparallel triplex-forming strategy. (b) Comparison of fluorescence intensities. "Mixture" refers to the AgNCs synthesized from the previously annealed mixture of the probe and the target. (c) HPLC separation of CC1_7C-based species. (d) Assessment of the selectivity of CC1_7C-AgNC probe. In all cases, DNA strand, silver nitrate and sodium borohydride concentrations were 5, 30, and 30 μM, respectively. The solutions contained 20 mM cacodylate buffer (pH 7.1), and 50 mM magnesium chloride. Measurements were conducted at 15 °C.

triplex structures, which are difficult to observe with other spectroscopic methods.

Declaration of competing interest

The authors declare the following financial interests/personal relationships which may be considered as potential competing interests: Raimundo Gargallo reports financial support was provided by Spain Ministry of Science and Innovation. Ramon Eritja reports financial support was provided by Marathon Foundation of Tv3. If there are other authors, they declare that they have no known competing financial interests or personal relationships that could have appeared to influence the work reported in this paper.

Acknowledgments

We thank funding from the Spanish *Ministerio de Ciencia e Innovación* (PID2023-146465NB-I00 and PID2020-118145RB-I00) funded by MCIN/AEI/10.13039/501100011033 and "ERDF A way of making Europe", and *La Marató* de TV3 Foundation (202110-30). Ana María San Millán (University of Barcelona) is thanked for her collaboration.

Appendix A. Supplementary data

Supplementary data to this article can be found online at https://doi.org/10.1016/j.saa.2024.125567.

Data availability

Data will be made available on request.

References

[1] R. Eritja, Nucleic acids triple helices, in: R. Eritja (Ed.), Nucleic Acids Chemistry. Modifications and Conjugates for Biomedicine and Nanotechnology, Walter de Gruyter GmbH, Berlin, 2021, pp. 187–230.
[2] C. Dagneaux, H. Gousset, A.K. Shchyolkina, M. Ouali, R. Letellier, J. Liquier, V. L. Florentiev, E. Taillandier, Parallel and antiparallel A*A-T intramolecular triple helices, Nucl. Acids Res. 24 (1996) 4506–4512, https://doi.org/10.1093/nar/24.22.4506.
[3] V. Noé, E. Aubets, A.J. Félix, C.J. Ciudad, Nucleic acids therapeutics using PolyPurine Reverse Hoogsteen hairpins, Biochem. Pharmacol. 189 (2021) 114371, https://doi.org/10.1016/j.bcp.2020.114371.
[4] S. Valiuska, A.M. Psaras, V. Noé, T.A. Brooks, C.J. Ciudad, Targeting MYC regulation with polypurine reverse hoogsteen oligonucleotides, Int. J. Mol. Sci. 24 (2022) 378, https://doi.org/10.3390/ijms24010378.
[5] A. Aviñó, C.S. Huertas, L.M. Lechuga, R. Eritja, Sensitive and label-free detection of miRNA-145 by triplex formation, Anal. Bioanal. Chem. 408 (2016) 885–893, https://doi.org/10.1007/s00216-015-9180-6.
[6] X. Zhu, Y. Liu, J. Yang, Z. Liang, G. Li, Gold nanoparticle-based colorimetric assay of single-nucleotide polymorphism of triplex DNA, Biosens. Bioelectron. 25 (2010) 2135–2139, https://doi.org/10.1016/j.bios.2010.02.017.
[7] F. Chen, Q. Lu, L. Huang, B. Liu, M. Liu, Y. Zhang, J. Liu, DNA triplex and quadruplex assembled nanosensors for correlating K^+ and pH in lysosomes, Angew. Chem. – Int. Ed. 60 (2021) 5453–5458, https://doi.org/10.1002/anie.202013302.
[8] P.-Y. Lin, R. Chi, Y.-L. Wu, J.A. Ho, Applications of triplex DNA nanostructures in sensor development, Anal. Bioanal. Chem. 414 (2022) 5217–5237, https://doi.org/10.1007/s00216-022-04058-8.
[9] J.P. Wilcoxon, B.L. Abrams, Synthesis, structure and properties of metal nanoclusters, Chem. Soc. Rev. 35 (2006) 1162–1194, https://doi.org/10.1039/B517312B.
[10] J.T. Petty, J. Zheng, N.V. Hud, R.M. Dickson, DNA-templated Ag nanocluster formation, J. Am. Chem. Soc. 126 (2004) 5207–5212, https://doi.org/10.1021/ja031931o.
[11] J. Sharma, H.-C. Yeh, H. Yoo, J.H. Werner, J.S. Martinez, A complementary palette of fluorescent silver nanoclusters, Chem. Commun. 46 (2010) 3280–3282, https://doi.org/10.1039/b927268b.
[12] B. Han, E. Wang, DNA-templated fluorescent silver nanoclusters, Anal. Bioanal. Chem. 402 (2012) 129–138, https://doi.org/10.1007/s00216-011-5307-6.
[13] I. Díez, R.H.A. Ras, Fluorescent silver nanoclusters, Nanoscale 3 (2011) 1963–1970, https://doi.org/10.1039/c1nr00006c.
[14] Z. Yuan, Y.-C. Chen, H.-W. Li, H.-T. Chang, Fluorescent silver nanoclusters stabilized by DNA scaffolds, Chem. Commun. 50 (2014) 9800–9815, https://doi.org/10.1039/C4CC02981J.
[15] M. Yang, L. Zhu, W. Yang, W. Xu, Nucleic acid-templated silver nanoclusters: a review of structures, properties, and biosensing applications, Coord. Chem. Rev. 491 (2023) 215247, https://doi.org/10.1016/j.ccr.2023.215247.
[16] H.-B. Wang, H.-Y. Bai, A.-L. Mao, T. Gan, Y.-M. Liu, Poly(adenine)-templated fluorescent Au nanoclusters for the rapid and sensitive detection of melamine, Spectrochim. Acta A Mol. Biomol. Spectrosc. 219 (2019) 375–381, https://doi.org/10.1016/j.saa.2019.04.075.
[17] N.-N. Wu, L.-G. Chen, H.-B. Wang, A sensitive fluorescence sensor for tetracycline determination based on adenine thymine-rich single-stranded DNA-templated copper nanoclusters, Appl. Spectrosc. 77 (2023) 1206–1213. https://opg.optica.org/as/abstract.cfm?URI=as-77-10-1206.
[18] S.Y. New, S.T. Lee, X.D. Su, DNA-templated silver nanoclusters: structural correlation and fluorescence modulation, Nanoscale 8 (2016) 17729–17746, https://doi.org/10.1039/C6NR05872H.
[19] M. Yang, X. Chen, Y. Su, H. Liu, H. Zhang, X. Li, W. Xu, The fluorescent palette of DNA-templated silver nanoclusters for biological applications, Front. Chem. 8 (2020). https://www.frontiersin.org/article/10.3389/fchem.2020.601621.
[20] J. Xu, X. Zhu, X. Zhou, F. Yeasmin, C. Ma, Recent advances in the bioanalytical and biomedical applications of DNA-templated silver nanoclusters, Trends Anal. Chem. 124 (2020) 115786, https://doi.org/10.1016/j.trac.2019.115786.
[21] K. Ma, Q. Cui, G. Liu, F. Wu, S. Xu, Y. Shao, DNA abasic site-directed formation of fluorescent silver nanoclusters for selective nucleobase recognition, Nanotechnology 22 (2011) 305502, https://doi.org/10.1088/0957-4484/22/30/305502.
[22] S.W. Yang, T. Vosch, Rapid detection of microRNA by a silver nanocluster DNA probe, Anal. Chem. 83 (2011) 6935–6939, https://doi.org/10.1021/ac201903n.
[23] M. Zhang, Y.Q. Liu, C.Y. Yu, B.C. Yin, B.C. Ye, Multiplexed detection of microRNAs by tuning DNA-scaffolded silver nanoclusters, Analyst 138 (2013) 4812–4817, https://doi.org/10.1039/c3an00666b.
[24] E. Shokri, M. Hosseini, F. Faridbod, M. Rahaie, Rapid pre-symptomatic recognition of tristeza viral RNA by a novel fluorescent self-dimerized DNA-silver nanocluster probe, RSC Adv. 6 (2016) 99437–99443, https://doi.org/10.1039/c6ra15199j.
[25] S. Javani, R. Lorca, A. Latorre, C. Flors, A.L. Cortajarena, Á. Somoza, Antibacterial activity of DNA-stabilized silver nanoclusters tuned by oligonucleotide sequence, ACS Appl. Mater. Interf. 8 (2016) 10147–10154, https://doi.org/10.1021/acsami.6b00670.
[26] J.F. García, D. Reguera, A. Valls, A. Aviñó, A. Dominguez, R. Eritja, R. Gargallo, Detection of pyrimidine-rich DNA sequences based on the formation of parallel and antiparallel triplex DNA and fluorescent silver nanoclusters, Spectrochim. Acta A Mol. Biomol. Spectrosc. 297 (2023) 122752, https://doi.org/10.1016/j.saa.2023.122752.
[27] T. Li, N. He, J. Wang, S. Li, Y. Deng, Z. Wang, Effects of the i-motif DNA loop on the fluorescence of silver nanoclusters, RSC Adv. 6 (2016) 22839–22844, https://doi.org/10.1039/C5RA22489F.
[28] R. Nagda, S. Park, I.L. Jung, K. Nam, H.C. Yadavalli, Y.M. Kim, K. Yang, J. Kang, P. W. Thulstrup, M.J. Bjerrum, M. Cho, T.-H. Kim, Y.H. Roh, P. Shah, S.W. Yang, Silver nanoclusters serve as fluorescent rivets linking hoogsteen triplex DNA and hairpin-loop DNA structures, ACS Nano 16 (2022) 13211–13222, https://doi.org/10.1021/acsnano.2c06631.
[29] A. Domínguez, R. Gargallo, C. Cuestas-Ayllón, V. Grazu, C. Fàbrega, S. Valiuska, V. Noé, C.J. Ciudad, E.J. Calderon, J.M. de la Fuente, R. Eritja, A. Aviñó, Biophysical evaluation of antiparallel triplexes for biosensing and biomedical applications, Int. J. Biol. Macromol. 264 (2024) 130540, https://doi.org/10.1016/j.ijbiomac.2024.130540.
[30] A. Aviñó, C. Cuestas-Ayllón, M. Gutiérrez-Capitán, L. Vilaplana, V. Grazu, V. Noé, E. Balada, A. Baldi, A.J. Félix, E. Aubets, S. Valiuska, A. Domínguez, R. Gargallo, R. Eritja, M.-P. Marco, C. Fernández-Sánchez, J. Martínez de la Fuente, C.J. Ciudad, Detection of SARS-CoV-2 virus by triplex enhanced nucleic acid detection assay (TENADA), Int. J. Mol. Sci. 23 (2022) 15258, https://doi.org/10.3390/ijms232315258.
[31] W.A. Kibbe, Oligo Calc: an online oligonucleotides properties calculator, Nucl. Acids Res. 35 (2007) W43–W46.
[32] S.S. Gaddis, Q. Wu, H.D. Thames, J. Digiovanni, E.F. Walborg, M.C. MacLeod, K. M. Vasquez, A web-based search engine for triplex-forming oligonucleotide target sequences, Oligonucleotides 16 (2006) 196–201, https://doi.org/10.1089/oli.2006.16.196.
[33] C.I. Richards, S. Choi, J.-C. Hsiang, Y. Antoku, T. Vosch, A. Bongiorno, Y.-L. Tzeng, R.M. Dickson, Oligonucleotide-stabilized Ag nanocluster fluorophores, J. Am. Chem. Soc. 130 (2008) 5038–5039, https://doi.org/10.1021/ja8005644.
[34] A. de la Hoz, A. Navarro, A. Aviñó, R. Eritja, R. Gargallo, Studies on the interactions of Ag (I) with DNA and their implication on the DNA-templated synthesis of silver nanoclusters and on the interaction with, RSC Adv. 11 (2021) 9029–9042, https://doi.org/10.1039/D1RA00194A.
[35] P. Kumar, A. Verma, S. Maiti, R. Gargallo, S. Chowdhury, Tetraplex DNA transitions within the human c- *myc* promoter detected by multivariate curve resolution of fluorescence resonance energy transfer, Biochemistry 44 (2005) 16426–16434, https://doi.org/10.1021/bi051452x.
[36] M. Vives, R. Gargallo, R. Tauler, Study of the intercalation equilibrium between the polynucleotide poly(adenylic)−poly(uridylic) acid and the ethidium bromide dye by means of multivariate curve resolution and the multivariate extension of the continuous variation and mole ratio methods, Anal. Chem. 71 (1999) 4328–4337, https://doi.org/10.1021/ac990131m.
[37] L. Bchara, R. Eritja, R. Gargallo, F. Benavente, Rapid and highly efficient separation of i-Motif DNA species by CE-UV and multivariate curve resolution, Anal. Chem. 95 (2023) 15189–15198, https://doi.org/10.1021/acs.analchem.3c01730.

[38] S. Ruiz-Castelar, A. Checa, R. Gargallo, J. Jaumot, Combination of chromatographic and chemometric methods to study the interactions between DNA strands, Anal. Chim. Acta 722 (2012) 34–42, https://doi.org/10.1016/j.aca.2012.02.005.
[39] M. Zuker, Mfold web server for nucleic acid folding and hybridization prediction, Nucl. Acids Res. 31 (2003) 3406–3415, https://doi.org/10.1093/NAR/GKG595.
[40] R.A. Dimitrov, M. Zuker, Prediction of hybridization and melting for double-stranded nucleic acids, Biophys. J. 87 (2004) 215–226, https://doi.org/10.1529/biophysj.103.020743.
[41] D. Schultz, K. Gardner, S.S.R. Oemrawsingh, N. Markešević, K. Olsson, M. Debord, D. Bouwmeester, E. Gwinn, Evidence for rod-shaped DNA-stabilized silver nanocluster emitters, Adv. Mater. 25 (2013) 2797–2803, https://doi.org/10.1002/adma.201204624.
[42] P. Mastracco, S.M. Copp, Beyond nature's base pairs: machine learning-enabled design of DNA-stabilized silver nanoclusters, Chem. Commun. 59 (2023) 10360–10375, https://doi.org/10.1039/D3CC02890A.
[43] J. Ma, H. Niu, S. Gu, The spatial organization of trace silver atoms on a DNA template, RSC Adv. 11 (2021) 1153–1163, https://doi.org/10.1039/D0RA08066G.
[44] A. Jain, G. Wang, K.M. Vasquez, DNA triple helices: biological consequences and therapeutic potential, Biochimie 90 (2008) 1117–1130, https://doi.org/10.1016/j.biochi.2008.02.011.
[45] R. Geczy, N.J. Christensen, K.K. Rasmussen, I. Kálomista, M.K. Tiwari, P. Shah, S. W. Yang, M.J. Bjerrum, P.W. Thulstrup, Formation and structure of fluorescent silver nanoclusters at interfacial binding sites facilitating oligomerization of DNA hairpins, Angew. Chem. Int. Ed. Engl. 59 (2020) 16091–16097, https://doi.org/10.1002/anie.202005102.
[46] S.M. Swasey, N. Karimova, C.M. Aikens, D.E. Schultz, A.J. Simon, E.G. Gwinn, Chiral electronic transitions in fluorescent silver clusters stabilized by DNA, ACS Nano 8 (2014) 6883–6892, https://doi.org/10.1021/nn5016067.